Control delivery of multiple growth factors to actively steer differentiation and extracellular matrix protein production

Damanik, F.F.R.; Verkoelen, N.; Blitterswijk, C. van; Rotmans, J.; Moroni, L.

Control Delivery of Multiple Growth Factors to Actively Steer Differentiation and Extracellular Matrix Protein Production

*Febriyani F. R. Damanik, Niels Verkoelen, Clemens van Blitterswijk, Joris Rotmans, and Lorenzo Moroni**

In tissue engineering, biomaterials have been used to steer the host response. This determines the outcome of tissue regeneration, which is modulated by multiple growth factors (GFs). Hence, a sustainable delivery system for GFs is necessary to control tissue regeneration actively. A delivery technique of single and multiple GF combinations, using a layer-by-layer (LBL) procedure to improve tissue remodeling, is developed. TGF-β1, PDGF-$\beta\beta$, and IGF-1 are incorporated on tailor-made polymeric rods, which could be used as a tool for potential tissue engineering applications, such as templates to induce the formation of in situ tissue engineered blood vessels (TEBVs). Cell response is analyzed in vitro using rat and human dermal fibroblasts for cellular proliferation, fibroblast differentiation, and extracellular matrix (ECM) protein synthesis. Results revealed a higher loading efficiency and control release of GFs incorporated on chloroform and oxygen plasma-activated (COX) rods. Single PDGF-$\beta\beta$ and IGF-1 release, and dual release with TGF-β1 from COX rods, showed higher cell proliferation when compared to COX rods alone. A substantial increase in α-smooth muscle actin (α-SMA) is also observed in GF releasing COX rods, with TGF-β1 COX rods providing the most pronounced differentiation. A significant increase in collagen and elastin synthesis is observed on all GF releasing COX rods compared to control, with COX rods releasing TGF-β1 and IGF-1 providing the highest secretion. TGF-β1 and IGF-1 releasing COX rods induced higher Glycosaminoglycan (GAG)/DNA amounts than the other GF releasing COX rods. As PDGF-$\beta\beta$ and TGF-β1/PDGF-$\beta\beta$ COX rods displayed the highest fibroblast attachment, these rods provided the highest total collagen and elastin production. The attractive results from efficiently incorporating single and multiple GFs on COX rods and their sustainable release to steer cellular behavior suggest a promising route to enrich the formation of in situ engineered tissues.

1. Introduction

The natural process of tissue regeneration in adult humans occurs during an injury and often represents a recapitulation of the developmental process. Regeneration is stimulated by the host immune response in the attempt to restore tissue structure and function. The degree of regeneration is deter-

mined by the host response eliciting a microenvironment in which the tissue will heal.[1] Hence, a promising approach for restoring tissue integrity and function is by replicating such biological environment and activating crucial regeneration pathways. For decades, tissue engineers have developed numerous biomaterials to initiate a suitable host response for cells to migrate, grow and induce tissue regeneration.[2,3]

Dr. F. F. R. Damanik, Prof. C. van Blitterswijk, Prof. L. Moroni
Tissue Regeneration Department
MIRA Institute for Biomedical Technology and Technical Medicine
University of Twente
Drienerlolaan 5, Zuidhorst 145, Enschede, NB 7522, The Netherlands
E-mail: l.moroni@maastrichtuniversity.nl

The ORCID identification number(s) for the author(s) of this article can be found under https://doi.org/10.1002/adbi.202000205.

Dr. F. F. R. Damanik, N. Verkoelen, Prof. C. van Blitterswijk, Prof. L. Moroni
Complex Tissue Regeneration Department
Maastricht University
MERLN Institute for Technology-Inspired Regenerative Medicine
Universiteitsingel 40, Maastricht 6229 ER, The Netherlands

Prof. J. Rotmans
Department of Nephrology
Leiden University Medical Center
Albinusdreef 2, Leiden 2333 ZA, The Netherlands

Previous studies have screened in vitro and in vivo surface modified polymeric rods, electing a specific physicochemical surface to induce a desirable host response creating a tissue-engineered blood vessel (TEBV) by using an in vivo bioreactor model.[4–6] The concept takes advantage of the foreign body response (FBR) developing a fibrocellular capsule composed of (myo)fibroblasts, macrophages, and foreign body giant cells. Subcutaneous implantation of a cylindrical polymeric rod originates a tube-shape tissue capsule, forming the basis for a TEBV.[7]

Introduction of biological mediators, such as growth factors (GFs) to directly orchestrate tissue regeneration, can further enhance the developed TEBV. Transforming growth factor beta (TGF-β) is involved in numerous tissue regeneration processes including inflammation, fibroblast proliferation, myofibroblast differentiation, angiogenesis, collagen synthesis and extracellular matrix (ECM) remodelling.[8] Platelet derived growth factor (PDGF) supports TGF-β, by recruiting fibroblast, stimulating angiogenesis, vessel maturation, as well as myofibroblast differentiation.[9] Moreover, insulin growth factor 1 (IGF-1) stimulates cell proliferation and production of ECM proteins. Recently, it has also been shown that IGF-1 increases myofibroblasts differentiation during wound healing in rats.[10]

Although seen as a promising approach to create a biological environment to instruct various cellular responses, GFs are soluble secreted polypeptides susceptible to degradation caused by denaturation, oxidation and proteolysis in vivo. PDGF has a short half-life of about 2 min when injected intravenously.[11] Similarly, TGF-β and IGF-1 have a short lifetime of a couple of minutes to 10–20 min, necessitating repetitive, high dose injections to induce a biological effect on the target tissue.[12,13] Moreover, the use of large quantities of GFs at once should be avoided as it may lead to pathological tissue formation at undesirable sites.[14–16] Hence, encapsulation of these GFs onto biomaterial substrates, protecting them from degradation, is crucial for its therapeutic efficiency. Despite layer-by-layer (LbL) systems have already been developed for the delivery of GFs,[17–19] we previously reported over a new LbL method to improve the loading of GFs efficiency. We showed controlled release, while still maintaining their biological functionalities.[20]

The complex cellular process of migration, proliferation, differentiation and protein secretion are typically dependant on the presence of specific spatio-temporal distribution of multiple GFs. Numerous studies have encouraged the combination of GFs sequentially released over single delivery.[21] For example, vascular endothelial growth factor (VEGF) and PDGF-$\beta\beta$ dual-delivery enhanced vessel size and maturity, when compared to VEGF alone.[22] In addition, combinatorial delivery of TGF-β1 and IGF-1 from poly(D, L-lactide) coating have been proven to enhance bone regeneration in bone induced titanium substrate.[23] Hence, developing a multiple delivery system to sequentially release TGF-β1, PDGF-$\beta\beta$, and IGF-1 from TEBV-inducing rods may provide the necessary enhancement for successful vascular tissue formation.

In the present study, we developed a dual delivery system of TGF-β1 and PDGF-$\beta\beta$, and TGF-β1 and IGF-1 onto TEBV-inducing rods based on LbL polyelectrolytes, and examined its biofunctionality in comparison to single delivery of GFs in vitro. We studied the influence of plasma treatment of the rods in combination with controlled surface topography provided by chemical etching on GFs incorporation efficiency in the LbL coatings. Cell proliferation, myofibroblast differentiation and production of ECM proteins such as glycosaminoglycan (GAG), collagen, and elastin were examined using a rat and human in vitro model to compare it to previous in vitro mimicking FBR studies aiming at the potential production of TEBVs. Ultimately, these modified rods could be also used as a tool for potential different in situ tissue engineering applications.

2. Results

2.1. Surface Modification and Activation on Polyelectrolyte Deposition

Figure 1 summarizes the methodology developed and used in this study to release dual growth factors and study their effect on fibroblasts activity. First, we investigate whether using chloroform etched surfaces alone, or in combination with oxygen plasma (COX) treatment provides a suitable substrate for efficiency growth factor loading. SEM images in **Figure 2**a-c showed oxygen plasma treated (Ox100) surface to provide submicrometer peaks, microporous structure in chloroform etched surface, and rough microporous structures accompanied by submicrometer peaks in COX treatment to PEOT/PBT rods. Surface topography and microporosity was very similar to what we have previously reported.[4] Additionally, ample surface charge is required to provide efficient polyelectrolyte deposition. Color-ionic staining using crystal violet for negatively charged surface or safranin for positively charged surfaces was performed (Figure S1, Supporting Information). Crystal violet staining indicated an increase in negative charge on COX surfaces compared to separate treatments, with chloroform treatment providing the least negative charge. None of the treatments did provide any surface positive charge (data not shown). When comparing loading capacity, COX surfaces provided the highest loading capacity compared to Ox100 and chloroform etched surfaces in all GFs (Figure 2d). Release rate profiles of single and dual GF loaded COX rods showed a sustained release of the incorporated GF over 21 days, reaching between 60% (for PDGF-$\beta\beta$) and 90% (for TGF-β1) cumulative release in case of single factor release, and between 60% (for PDGF-$\beta\beta$) and 80% for (for TGF-β1 and IGF-1) cumulative release in case of dual factors release, approximately (Figure 2e,f). For single factor release, this corresponded to $\approx$6 ng mL^{-1} at day 1 and 27 ng mL^{-1} at day 10, when the plateau was reached for TGF-β1. Similarly, PDGF-$\beta\beta$ release was $\approx$6 ng mL^{-1} at day 1 and 19 ng mL^{-1} at day 14, when the plateau was reached; IGF-1 release was $\approx$72 ng mL^{-1} at day 1 and 340 ng mL^{-1} at day 14, when the plateau was reached. For dual factors release, this corresponded to $\approx$5 ng mL^{-1} of released TGF-β1, 3 ng mL^{-1} of released PDGF-$\beta\beta$, and 40 ng mL^{-1} of released IGF-1 at day 1. Plateau was reached around day 14 in all conditions, with released values of $\approx$19 ng mL^{-1} for PDGF-$\beta\beta$, 320 ng mL^{-1} for IGF-1, and between 22 and 26 ng mL^{-1} for TGF-β1 when in combination with PDGF-$\beta\beta$ or IGF-1, respectively.

**ADVANCED
SCIENCE NEWS**
www.advancedsciencenews.com
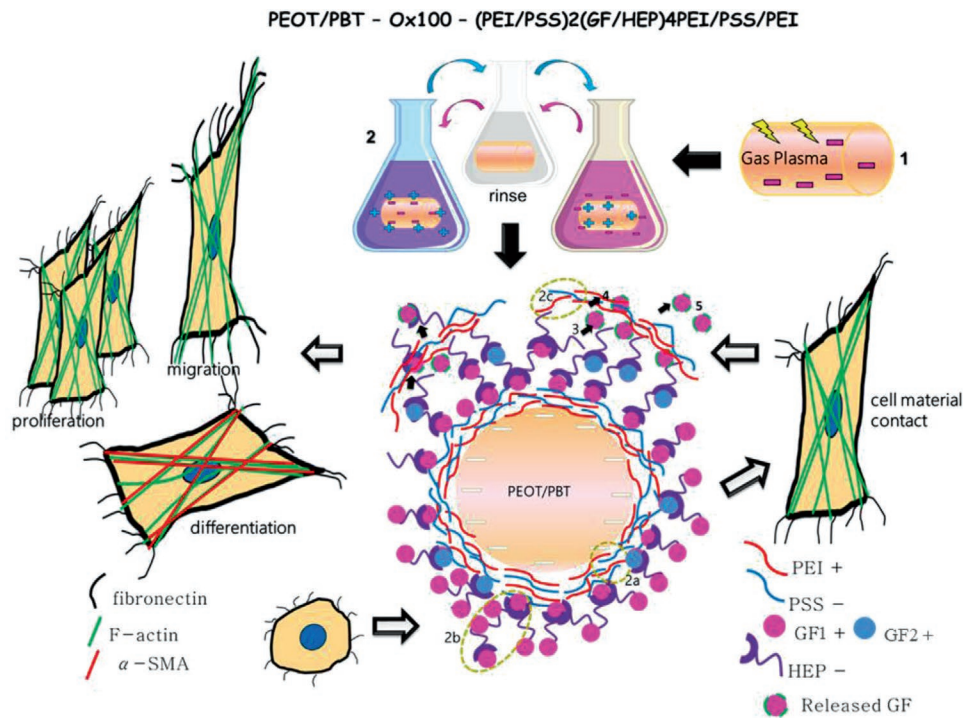
**ADVANCED
BIOLOGY**
www.advanced-bio.com

Figure 1. Schematic overview of single (GF1) and dual (GF2) GF-LBL methodology to assess their effect on fibroblasts seeded on the LBL implants. 1) The fabricated polymeric implant rod was first gas plasma treated to create a negatively charged surface for polyelectrolyte deposition. 2) Polyelectrolyte deposition step comprises of incubating the implant to positively and negatively charged solutions of PEI and PSS (2a, first 4 layers), GF and HEP (2b, next 8 layers) and again PEI and PSS (2c, for the last 3 layers), for the single GF releasing implants. In case of dual GF releasing implants, GF1 and GF2 were alternated in the 8 layers. 3–5) In culture medium, GF1 and GF2 start to be released from the LBL assembly, diffusing through the top PEI-PSS-PEI layer. After seeding fibroblasts on LBL implant, their migration, proliferation and differentiation is actively steered by GF1 and GF2 local release. Adapted with permission.[20] Copyright 2019, RSC.

Considering that values at plateau corresponds to cumulative release and that the release rate was close to a linear rate, we can conclude that all growth factors were released in time at concentrations close to physiological values when considering vasculogenesis for TEBV applications.[26]

Mechanical properties remained unchanged after surface treatment. The bending modulus of the rods was 137 ± 8 MPa for surface treated rods and 138 ± 8 MPa for untreated rods.

2.2. Effect on Cell Proliferation of GF Releasing COX Rods

To understand the proliferative effect of GF releasing COX rods during the initial week of FBR, DNA assay was conducted up to day 7 (**Figure 3**). Single and dual PDGF-$\beta\beta$ releasing COX rods provided a substantial increase in nRDF proliferation between day 1 and day 4 compared to all GF releasing and non-releasing rods (control). In contrast, single and dual IGF-1 releasing COX rods showed a decrease in nRDF proliferation compared to control, though not statistically significant. A substantial decrease in nRDF proliferation rate was seen in all COX rods between day 4 and day 7, with fibroblast attached to IGF-1 releasing COX rods being the highest in cell proliferation. nRDF attached to PDGF-$\beta\beta$ releasing COX rods at this later time point still provided a statistically higher proliferation rate than control. HDF attached to GF releasing rods and control rods displayed a different proliferation profile. The combinatory effect of TGF-β1

and IGF-1 provided a statistically significant increase in HDF proliferation between day 1 and day 4, while IGF-1 alone decreased proliferation rate, though not statistically significant. This combinatory effect releasing multiple GFs was also seen in TGF-β1/PDGF-$\beta\beta$ COX rods, though not as significant as TGF-β1/IGF-1 COX rods. Amongst single GF releasing COX rods, HDF attached to PDGF-$\beta\beta$ releasing COX rods provided the highest proliferation rate. Similar to nRDF, HDF proliferation analysis between day 4 and day 7 displayed a decrease in proliferation rate with single and dual PDGF-$\beta\beta$ COX rods, when compared to proliferation between day 1 and day 4, providing highest proliferation rate.

2.3. Cell Morphology and Myofibroblast Differentiation

nRDFs and HDFs displayed different morphology on different GF releasing rods and control rods at day 1 (**Figure 4**). Cells found in TGF-β1 COX rods seemed to be more spread and squared compared to PDGF-$\beta\beta$ COX rods, which were more narrow and elongated. Similar to PDGF-$\beta\beta$ rods, cells found on IGF-1 COX rods exhibited spread and elongated morphology. Combinatory effect of dual GF release provided a mix between both spread and elongated morphology of the cells attached. When quantifying cell circularity, these observations were confirmed with values spanning from 0.37 ± 0.1 for unmodified rods to 0.45 ± 0.22 for PDGF-$\beta\beta$ COX rods, and intermediate

**ADVANCED
SCIENCE NEWS**

www.advancedsciencenews.com
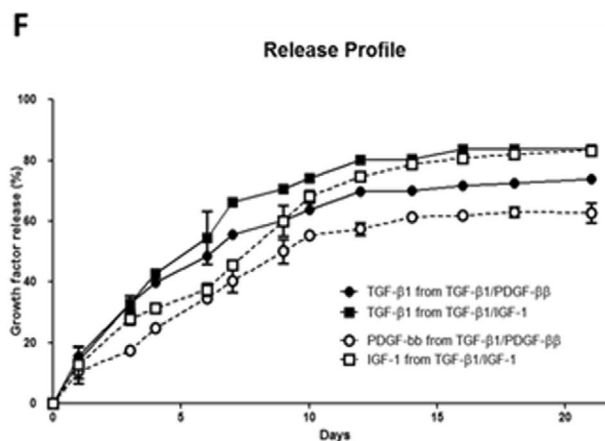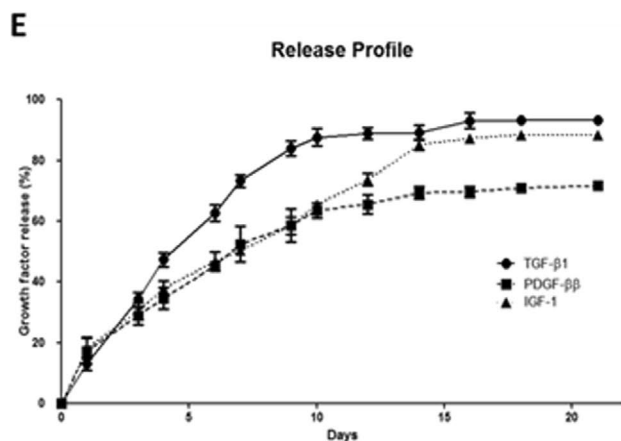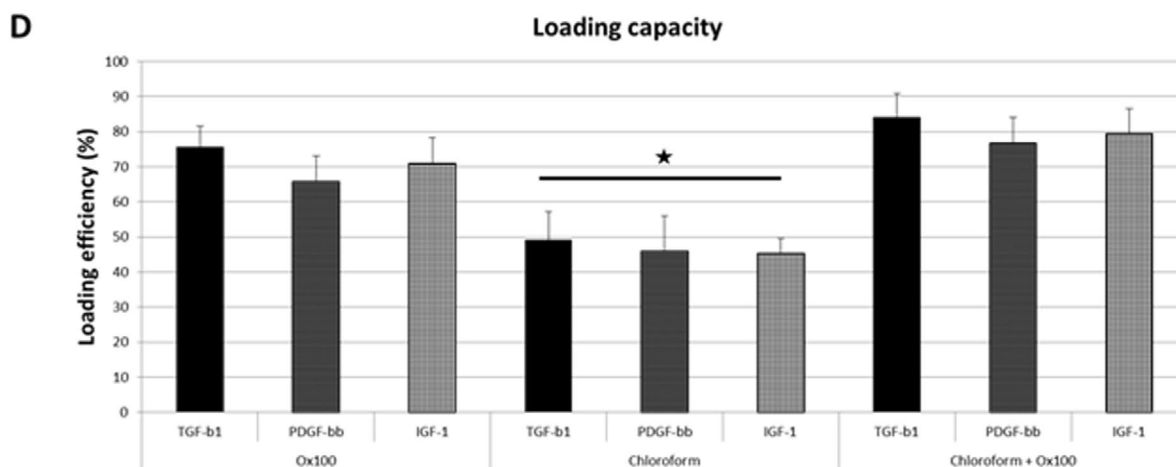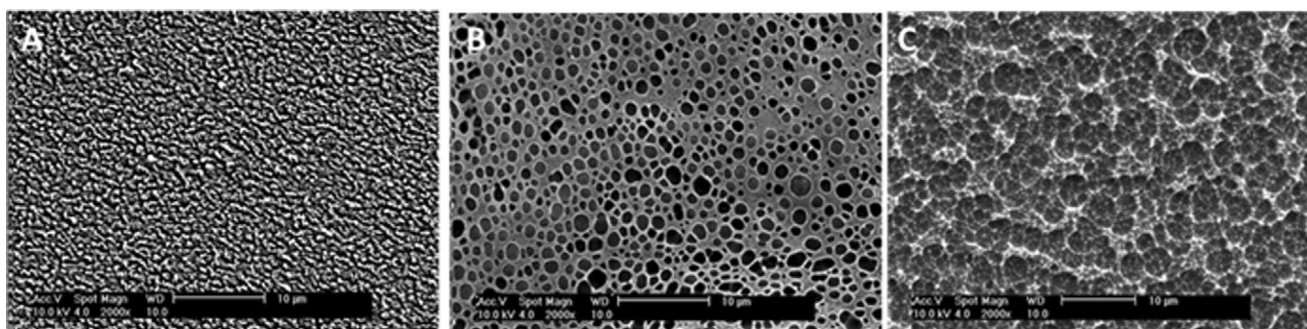
**ADVANCED
BIOLOGY**

www.advanced-bio.com

Figure 2. Surface modification and activation on GF incorporation. a–c) SEM images of PEOT/PBT surfaces after a) oxygen plasma, b) chloroform etching, and c) combination of chloroform etching and oxygen plasma. Scale bar: 10 μm. d) Comparison of PEOT/PBT surfaces on loading capacity of GFs, indicating a slight increase in loading efficiency for combination of chloroform and oxygen etched surfaces compared to oxygen plasma treated surfaces alone. A statistically significant difference (* $p < 0.05$) was seen in oxygen plasma treated surfaces alone and combination with chloroform compared to chloroform etched alone. e,f) Release rate profiles were measured for e) single and f) dual GF incorporation up to day 21, showing a sustainable release. All data are shown as mean ± s.d. ($n = 3$), if not stated otherwise.

values in all other conditions. GF releasing COX rods were further examined for their potential effect on myofibroblast differentiation and the state of attached cells actin fibres.

In addition to SEM analysis, immunochemistry staining revealed a population of fibroblasts that differentiated to myofibroblasts and actin fibres analysis (**Figure 5**). In nRDF cultures,

released TGF-β1 provided a substantial trigger for myofibroblast differentiation, as seen by the highly expressed α-SMA cells attached to TGF-β1 and TGF-β1/IGF-1 COX rods. At day 4 and day 7, cells attached to TGF-β1 COX rods displayed highly spread morphology and pronounced stressed actin fibres. The majority of cells found in IGF-1 COX rods were more stretched
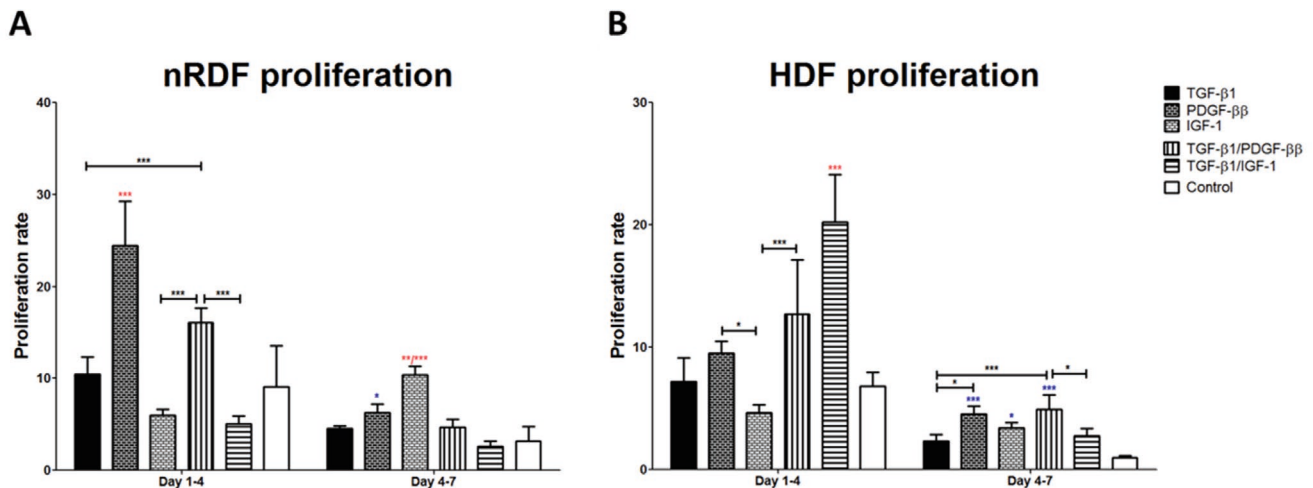
Figure 3. Cell proliferation rate of nRDF and HDF. Different COX rods are represented by different bar patterns. Proliferation rate is calculated by normalizing the DNA content of each group at day 4 to the DNA content of the same group at day 1. Similarly, the DNA content of each group at day 7 was normalized to the DNA content of the same group at day 4. Data are shown as mean ± s.d. ($n = 3$). a) nRDF proliferation rate between day 1 and 4 (early time point) displayed a higher proliferation rate compared to proliferation between day 4 and 7 (late time point). nRDF attached to PDGF-$\beta\beta$ COX rods provided the highest early time point proliferation rate, and IGF-1 COX rods for later time point (** $p < 0.01$ in comparison to PDGF-$\beta\beta$, *** $p < 0.001$ for all the other COX rods). b) Similarly, HDF proliferation rate at later time point decreased from early time point. TGF-β1/IGF-1 COX rods provided the highest proliferation rate between day 1 and day 4, while PDGF-$\beta\beta$ and TGF-β1/PDGF-$\beta\beta$ provided the highest proliferation rate between day 4 and day 7. DNA assay statistics were done using One-way Analysis of Variance (ANOVA) with Bonferroni's multiple comparison test ($p < 0.05$). Blue stars (*$p < 0.05$, ** $p < 0.01$, *** $p < 0.001$) indicate statistical significances in comparison to control, red stars indicate the highest proliferation rate found in all COX rod type, while black stars evaluate statistical differences between the different COX rods.

with stressed actin fibres at day 4, than at day 7. A combinatory effect from TGF-β1/IGF-1 COX rods provided a mixture of less and more pronounced stress actin fibres and spread out morphology at day 7. PDGF-$\beta\beta$ released from PDGF-$\beta\beta$ and TGF-β1/PDGF-$\beta\beta$ COX rods induced less myofibroblast differentiation, as shown by the low α-SMA expression, yet higher than control with no GF. Cells found in TGF-β1 COX rods had the highest α-SMA expression in day 4 HDF cultures. Though α-SMA expression from HDF found in PDGF-$\beta\beta$, IGF-1, TGF-β1/PDGF-$\beta\beta$ and TGF-β1/IGF-1 COX rods were similar to control rods at day 4, more prominent α-actin stress fibres were seen on all GF releasing COX rods. The release of TGF-β1 and IGF-1 seemed to trigger a more spread cell morphology for both time points. At day 7, the expression of α-SMA increase in all GF releasing COX

rods, with single release of TGF-β1 and with combinatory effect of PDGF-$\beta\beta$ and IGF-1, stimulated prominent actin stress fibres and higher expression of α-SMA compared to control rods.

2.4. GF Releasing COX Rod Effect on GAG, Collagen, and Elastin Expression

Secreted ECM proteins were quantified to analyze GF releasing COX rods capability to stimulate GAG, collagen and elastin secretion (**Figures 6–8**, Figures S3 and S4, Supporting Information). TGF-β1 COX rods stimulated nRDF to secrete the highest GAG/DNA at all measured time points (Figure 6). This was followed by high GAG/DNA production from nRDF
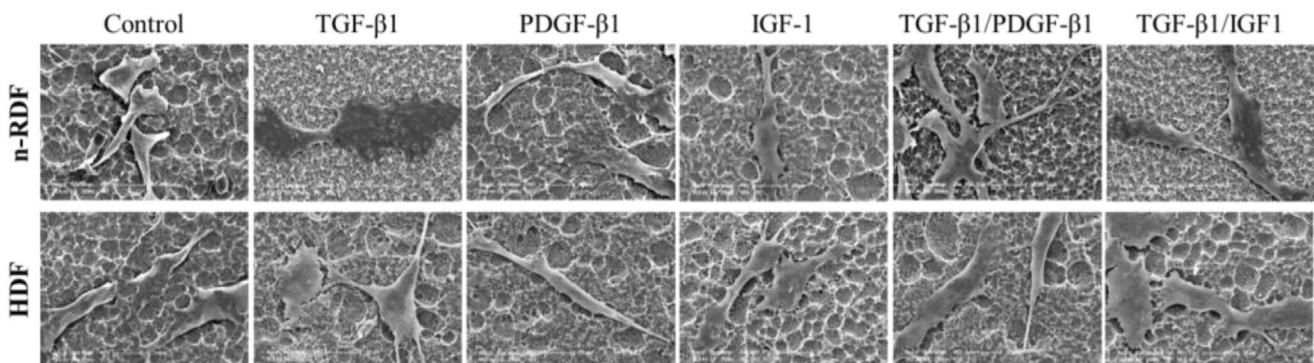
Figure 4. SEM image of cell morphology at day 1. Top row display nRDFs, while bottom row exhibit HDFs, attached to control and GF releasing COX rods. Cells on TGF-β1 COX rods showed a spread, square-like structure, while cells on IGF-1 quite spread morphology, and PDGF-$\beta\beta$ presented an elongated shape. Cell attached to TGF-β1/PDGF-$\beta\beta$ and TGF-β1/IGF-1 COX rods showed both characteristics of spread and elongated morphology. Scale bar: 20 µm.

**ADVANCED
SCIENCE NEWS**
www.advancedsciencenews.com

**ADVANCED
BIOLOGY**
www.advanced-bio.com

Figure 5. Immunostaining of cell actin fibres and α-SMA. Fluorescent images show α-SMA (green), phalloidin (red) and dapi (blue) immuno-stained cells attached to different COX rod types. Immunostaining images of a–l) nRDF at a–f) day 4 and g–l) day 7, show higher α-SMA ex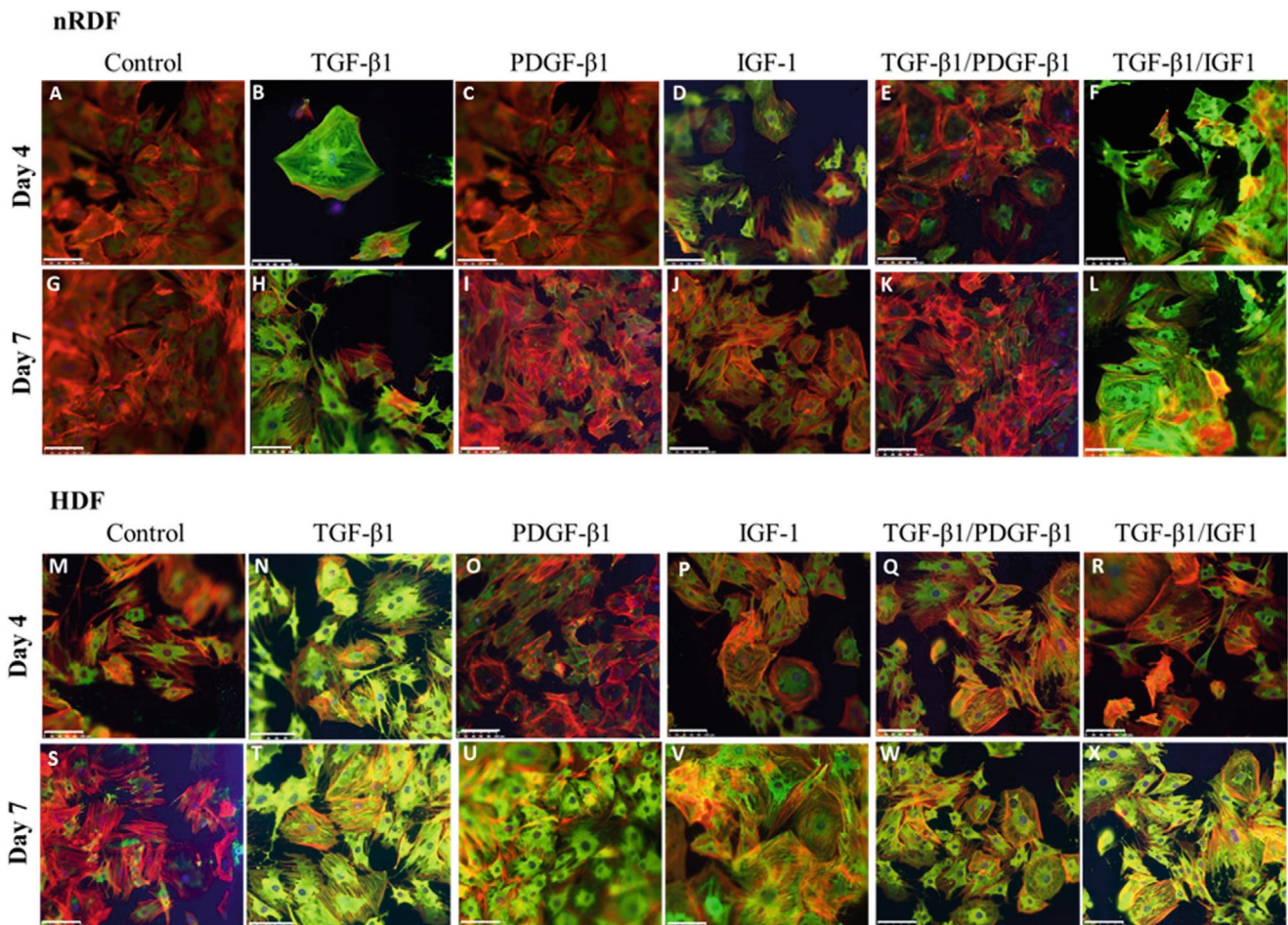pression on cells attached to TGF-β1 and TGF-β1/IGF-1 COX rods compared to PDGF-$\beta\beta$, IGF-1, TGF-β1/PDGF-$\beta\beta$ and control. m–x) Immunostaining of HDF at m–r) day 4, showed the highest population of α-smooth muscle actin positive cells on TGF-β1 COX rods and s–x) increase in α-smooth muscle actin positive cells on GF releasing COX rods compared to control at day 7. Scale bar: 100 µm.

found in PDGF-$\beta\beta$ COX rods at day 1, IGF-1 COX rods at day 4, and TGF-β1/IGF-1 COX rods at day 7, all significantly higher than control rods. A quite similar trend of high GAG secretion was seen in HDF cultures for the response to PDGF-$\beta\beta$ release from TGF-β1/PDGF-$\beta\beta$ COX rods at day 1 and IGF-1 releasing COX rods at day 4 and 7. Also in all measured time points, TGF-β1 COX rods elicited the highest GAG/DNA production in HDF cultures compared to all the other GF releasing COX rods. Nevertheless, only HDF attached to TGF-β1 and TGF-β1/PDGF-$\beta\beta$ COX rods at day 1 provided a significant increase in GAG/DNA amount compared to control.

TGF-β1 COX rods provided a significantly stable increase in collagen secretion per cell in nRDF cultures at all measured time points compared to control (Figure 7). The highest collagen production per cell was seen in IGF-1 COX rods at day 4. A combinatory effect of IGF-1 with TGF-β1 was seen at day 7, providing the highest collagen secretion per cell. All GF releasing COX rods provided statistically a significant increase in collagen secretion per cell and in total collagen secretion per

COX rod at all measured time points compared to control. The highest total collagen production was seen in TGF-β1/PDGF-$\beta\beta$ COX rods at all measured time points. Similar to nRDFs, HDFs secreted a stable significant increase of collagen per cell on TGF-β1 COX rods when compared to control, providing the highest secretion at all measured time points. Additionally, HDFs attached to IGF-1 COX rods at day 7 exhibited the second highest collagen per cell secretion. All GF releasing COX rods in HDF culture, with exception to TGF-β1/IGF-1, stimulated statistically a significant increase in collagen secretion per cell. Significantly higher total collagen secretion was seen for PDGF-$\beta\beta$ COX rods when compared to control at day 4, and highest secretion at day 7.

Single release of TGF-β1 and IGF-1, and dual release of TGF-1/IGF-β1 stimulated a significantly higher elastin secretion per cell on day 4 nRDF cultures. TGF-β1/IGF-1 COX rods provided the highest elastin per cell secretion on day 7 nRDF cultures (Figure 8). At day 7, nRDFs attached to all GF releasing COX rods provided a significant increase in elastin per cell production when compared to control, leading to
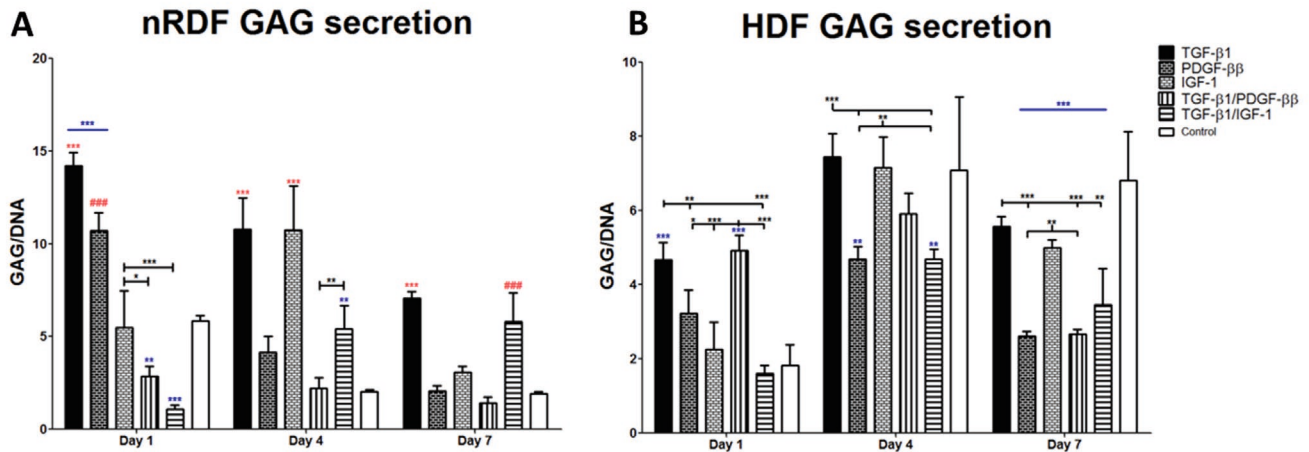
Figure 6. GAG measurement normalized by number of cells attached at day 1, 4, and 7. Different COX rods are represented by different bar patterns. Data are shown as mean ± s.d. ($n = 3$). a) GAG secretion per DNA was highest in nRDFs attached to TGF-β1 COX rods in all time points, and IGF-1 COX rods at day 4, followed by PDGF-$\beta\beta$ COX rods at day 1 and TGF-β1/IGF-1 COX rods at day 7. b) TGF-β1 COX rods stimulated the highest GAG/DNA production in HDFs attached to GF releasing COX rods. A significant increase in GAG/DNA production was only seen on HDFs attached to TGF-β1 and TGF-β1/PDGF-$\beta\beta$ COX rods compared to control. Blue stars (*$p < 0.05$, ** $p < 0.01$, *** $p < 0.001$) indicate statistical significances in comparison to control, red stars indicate the highest secretion found in all COX rod type, with red # showing second best, while black stars evaluate statistical differences between the different COX rods.

substantial increase in total elastin amount. PDGF-$\beta\beta$ and TGF-β1/PDGF-$\beta\beta$ COX rods stimulated the highest total elastin amount in nRDF cultures at day 7. In HDF cultures, PDGF-$\beta\beta$, IGF-1 and TGF-β1/PDGF-$\beta\beta$ COX rods displayed a significantly higher elastin secretion per cell at day 4. This supports the significant increase seen in total elastin production from HDF cultured in PDGF-$\beta\beta$, IGF-1 and TGF-β1/PDGF-$\beta\beta$ COX rods. At day 7, all GF releasing COX rods stimulated a significantly higher total elastin production compared to control.

3. Discussion

In this study, we evaluated the loading efficiency of single and multiple GFs on TEBV-inducing rods, and the effect of their controlled release on cellular behaviour to enhance the function of cells crucial for TEBV formation. A previously developed LBL method[20] introduced a loading capacity higher than the supposedly "high density drug loading," which is known to range from 10–40%.[27] The combination of this method with TEBV-inducing rods, which we have shown in previous studies
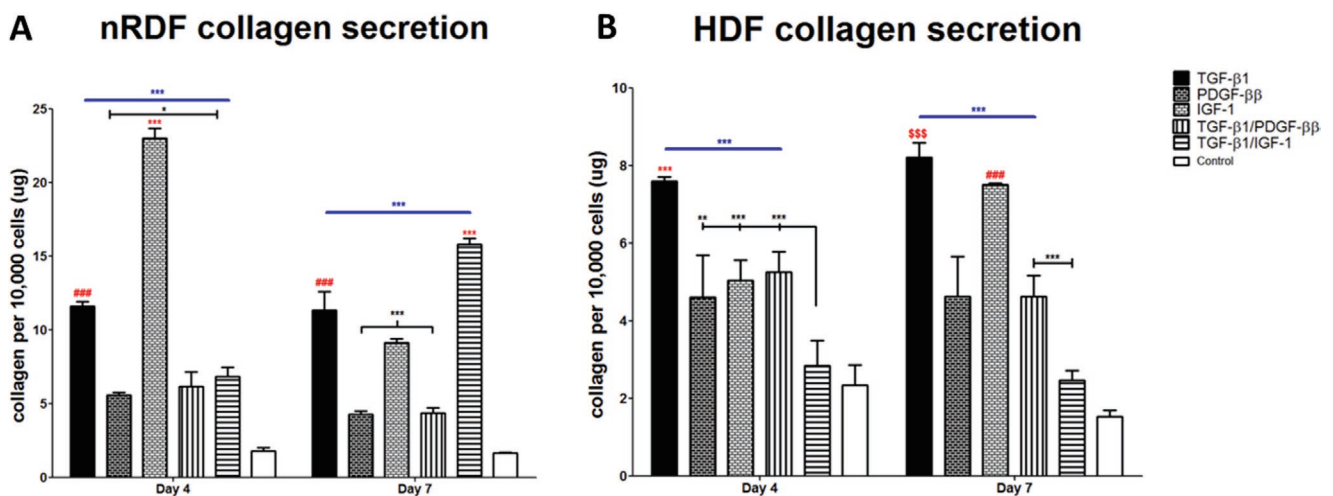

Figure 7. Collagen secretion per cells. Different COX rods are represented by different bar patterns. Data are shown as mean ± s.d. ($n = 3$). a) All GF releasing COX rods provided a statistically higher collagen secretion per cell compared to control. Collagen secretion per cells was significantly higher in TGF-β1 COX rods compared to control at day 4 and 7. Highest collagen secretion per cell was seen in IGF-1 COX rods at day 4, and TGF-β1/IGF-1 at day 7. b) All GF releasing COX rods provided a statistically higher collagen secretion per cell compared to control. Highest collagen secretion per cell was found in TGF-β1 COX rods at day 4 and 7, followed by IGF-1 COX rods at day 7. Blue stars (*$p < 0.05$, ** $p < 0.01$, *** $p < 0.001$) indicate statistical significances in comparison to control, red stars indicate the highest secretion found in all COX rod type, with red $ showing significance to all except one COX rod type and # showing second best, while black stars evaluate statistical differences between the different COX rods.
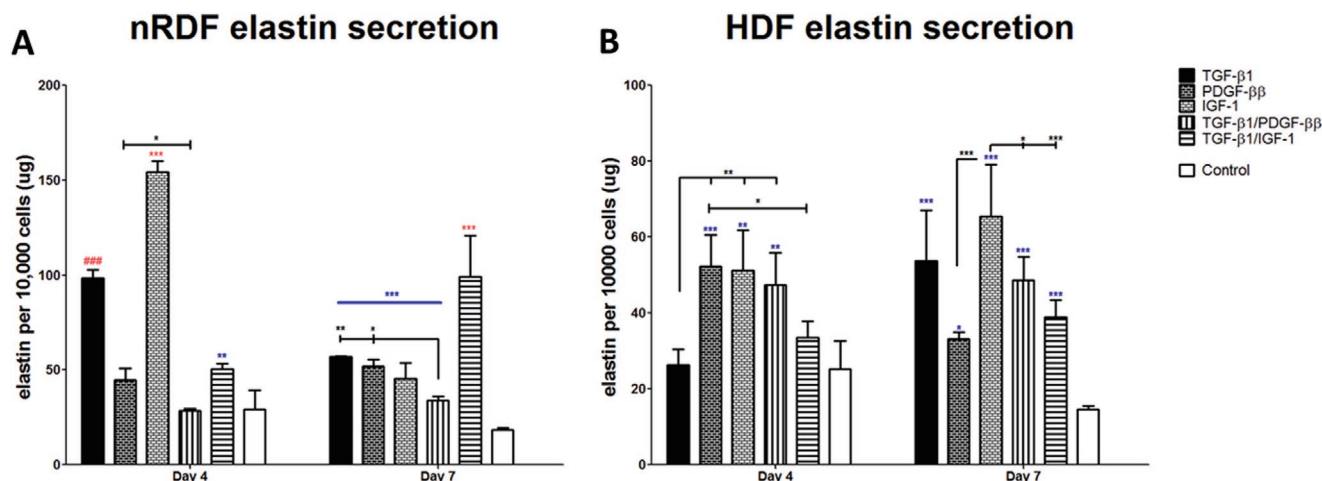
Figure 8. Elastin secretion per cells. Different COX rods are represented by different bar patterns. Data are shown as mean ± s.d. ($n = 3$). a) All GF releasing COX rods provided a statistically higher elastin secretion per cell compared to control at day 7, while only statistically higher in TGF-β1, IGF-1, and TGF-β1/IGF-1 COX rods at day 4. Highest elastin secretion per cell was seen in IGF-1 COX rods at day 4, and TGF-β1/IGF-1 at day 7, and second best in TGF-β1 at day 4. b) All GF releasing COX rods provided a statistically higher elastin secretion per cell compared to control at day 7 and only PDGF-$\beta\beta$, IGF-1, and TGF-β1/PDGF-$\beta\beta$ COX rods at day 4. Blue stars (*$p < 0.05$, ** $p < 0.01$, *** $p < 0.001$) indicate statistical significances in comparison to control, red stars indicate the highest secretion found in all COX rod type, with red # showing second best, while black stars evaluate statistical differences between the different COX rods.

to support the fabrication of a TEBV in situ,[5,7,28,29] requires a suitable substrate for efficient GF multilayer deposition. Here, we showed a higher loading capacity of this LBL method on surface activated TEBV-inducing rods by oxygen plasma treatment in comparison to PEOT/PBT oxygen plasma treated rods and smooth TEBV-inducing rods. PEOT/PBT, and in particular 300PEOT55PBT45, has been chosen due to the favourable physicochemical properties of this biodegradable copolymer family for drug release and tissue regeneration application. The specific copolymer used in this study is expected to degrade in a time frame between 2 and 4 years after implantation.[30,31] As previously shown,[20] PEI and PSS have been chosen among conventional polyelectrolytes used in LbL approaches to provide sufficient initial charge for the multilayer deposition, whereas heparin as a counter polyelectrolyte known to maintain GFs bioactivity by protecting their ligands. The combination of these polyelectrolytes is known to support a sustained release governed by diffusion and erosion through a Korsmeyer–Peppas model.[32,33]

An increase in surface area, due to incorporation of nanowires[34] or graphene oxide[35] have been shown to increase loading capacity of incorporated drugs. Hence, the increase in surface area after chloroform etching, creating porous structures,[4] followed by additional peak structures from oxygen plasma treatment could be the reason for higher loading capacity in COX rods.[36] Moreover, as the substrate charge is a crucial parameter in loading capacity, highly charged COX substrate may enhance loading capacity.[37] Incorporation of GFs through LBL may lead to an increased GF physicochemical stability.[36] Various drugs have been adsorbed and encapsulated by polyelectrolyte multilayer films on porous structures for sustained drug delivery.[19,38,39] Although drug release has been known to be directly proportional to solid surface area,[40] the etched porous topography provide additional inclusion of incorporated GF, resulting in a sustainable control release.

Growth factors have been known to induce a mitogenic effect on fibroblasts. PDGF-$\beta\beta$ is a pleiotropic growth factor regulating various cell functions, including proliferation.[41] Elevated cellular proliferation rate on PDGF-$\beta\beta$ releasing COX rods is to be expected. Nishiyama et al.[42] showed PDGF-$\beta\beta$, endothelial growth factor (EGF), basic fibroblast growth factor (bFGF) and TGF-β1 effect on quiescent HDF, inducing proliferation even in confluent cultures. Although the other GFs did not stimulate proliferation in cell-matrix inhibition cultures, PDGF-$\beta\beta$ mitogenic effect was still observed. Although PDGF-$\beta\beta$, EGF and bFGF could induce HDF proliferation in low serum conditions, a lack of mitogenic effect of TGF-β1 was noted. Various studies have shown debatable results concerning TGF-β1 mitogenic effect on fibroblasts and seemed to be influenced by the different fibroblast properties residing in different tissue and species. TGF-β1 has been shown to enhance the proliferation of renal, pulmonary and dermal fibroblasts,[43–46] but to inhibit the proliferation of luteal, oral, and colonic fibroblasts.[47–49] However, mitogenic inhibition or stimulation is also dependant from TGF-β1 concentration,[50] with studies showing maximal cell proliferation at 5 ng mL^{-1} of TGF-β1, which was released here and in previous LBL studies.[51,52] Yet, targeted cell number exposed to a specific GF concentration and surface substrate may also provide variance to cellular response, steering enhancement to ECM production instead.[53] Nevertheless, the combinatory influence of other GFs including PDGF-$\beta\beta$ and IGF-1 have been known to enhance cell proliferation. Studies of mitogenic improvement were observed when combining the effect of TGF-β1 and PDGF-$\beta\beta$ in quiescent HDFs[42] or TGF-β1 and IGF-1 in nucleus pulposus cells.[54] Similarly, our results displayed dual release of TGF-β1 with either PDGF-$\beta\beta$ or IGF-1 able to steer cell response to enhance cell proliferation.

At the end stage of tissue regeneration after a biomaterial implantation, the residing cells become quiescent, producing a limited amount of ECM proteins,[55] as also seen from the

**ADVANCED
SCIENCE NEWS**
www.advancedsciencenews.com

**ADVANCED
BIOLOGY**
www.advanced-bio.com

fibroblastic cells found in TEBV-inducing rods in vivo.[5] Sustainable release of GFs can further activate these fibroblastic cells to secrete a substantial amount of ECM proteins.[56] The majority of most ECM is composed of an interlocking mesh of fibrous proteins, such as collagen and elastin, and GAGs. Generally, TGF-β1 and IGF-1 release provided an increase in cell secretion of GAG in nRDF, and in HDF, though only at day 1. Previous studies displayed supporting results, with elevated cardiac fibroblast GAG levels after TGF-β1 incubation accompanied with mechanical stretch,[57] and higher production of GAG in chondrocytes due to TGF-β1 released from microspheres[58] or IGF-1 incorporation.[59] Combinatory effect of TGF-β and IGF-1 on GAG was more pronounced at later culture days, supporting Osch et al. results of higher GAG and collagen production.[60]

Collagen provides an essential role in sustaining ECM structural integrity, as well as its biological and mechanical functionality. Induction of collagen production was highly modulated by GFs, in which the release of TGF-β1, PDGF-$\beta\beta$, IGF-1 and their combination from TEBV-inducing rods further increased cell secretion of collagen, as previously seen in other studies.[8–10] Moreover, cell morphology has been known to correlate with cellular function.[61] Ivarsson et al. showed that round and spread cells induce collagen type I production.[62] These types of cells were vastly found in TGF-β1 COX rods, followed by IGF-1 COX rods, both with prominent actin stress fibers representing proto-myofibroblasts.[63] Introduction of PDGF-$\beta\beta$, however, replaced the cell spreading stimulus for direct collagen secretion, and instead stimulated cell elongation,[62] as similarly seen in our SEM results. Furthermore, collagen deposition is dose dependent to TGF-β1 concentration,[64] and can be altered by additional growth factor incorporation. A week exposure of dual release TGF-β1/IGF-1 COX rods stimulated a significantly higher collagen production, higher than TGF-β1 and IGF-1 alone in nRDF, suggesting the additive value of multiple GF release. Similarly, Daian et al.[65] showed TGF-β1 and IGF-1 co-induction to increase ECM proteins, collagen type I, fibronectin, and plasminogen activator inhibitor-1 and provide a higher synergistic stimulation, of 25-fold, compared to 10- and 2-fold basal activity from TGF-β1 or IGF-1 alone, respectively. Grotendorst et al.[66] supported this combinatory effect, in which TGF-β and IGF-1 together provided an additive value to collagen synthesis in renal fibroblast.

Secretion of collagen can be associated to the presences of myofibroblast differentiation in GF releasing COX rods, as some studies have reported up to 60% reduction of α-SMA expression by blocking endogenous TGF-β expression, leading to decrease in collagen production.[67] Moreover, Grotendorst et al.[66] observed a close relation to myofibroblast differentiation and induction of collagen synthesis. Immunostaining results displayed higher myofibroblast differentiation in COX rods releasing TGF-β1, followed by IGF-1. This is to be expected as TGF-β1 and IGF-1 have been known to be upregulated in myofibroblasts at sites of fibrosis.[48] Santiago et al.[64] has shown in vitro and in vivo the increase in α-SMA to be dose dependent, with more abundant α-SMA bundles found in more concentrated TGF-β1 areas. The delayed increase in myofibroblast differentiation in HDF is supported by Lederle et al.,[9] who observed a direct contribution of PDGF-$\beta\beta$ to α-SMA induction by stimulating a strong dose-dependent increase in

α-SMA-positive HDF. Nevertheless, the delay and lower expression of α-SMA from single and dual release PDGF-$\beta\beta$ COX rods, could explain the significant difference in collagen secretion of TGF-β1 and IGF-1 releasing COX rods.

Biomaterials implanted for vascular tissue replacement are required to induce a significant amount of collagen and elastin for mechanical strength and elasticity of the newly formed tissue. Elastin is a very crucial structural and regulatory matrix protein for soft tissue, especially for blood vessels, and has been known as the missing link in many vascular tissue engineering applications.[68] Here, we further improved elastin production by GF incorporation to TEBV-inducing rods, in which after a week exposure to either TGF-β1, PDGF-$\beta\beta$, IGF-1 and their combination, secreted a significant increase of total elastin and elastin per cell in both rat and human dermal fibroblast. The use of heparin as the counter polyelectrolyte of loaded GF could further enhance elastin secretion. In fact, depending on the growth state of the targeted cells, heparin has been known to induce elastogenesis.[69] Generally, the highest cell secretion of elastin was seen in COX rods releasing single and dual TGF-β1 and IGF-1, which could be highly expected as both IGF-1[70] and TGF-β1[71,72] have been observed to enhance elastin secretion.

In this study, we have successfully shown a strategy to deliver multiple growth factors from a polymeric rod device that could act as a template for in situ fabrication of a TEBV. Following this overarching goal, we aimed at understanding in a simple and simplified in vitro model how the released growth factors could influence the response of fibroblasts as one of the main cell population that would come into contact with the implanted polymeric rods. Future studies should aim at further dissecting the role of other cell types involved in the FBR such as macrophages, T regulatory cells, and endothelial cells. This would allow to more closely mimic the cellular microenvironment that would be present in vivo. We focused here on early response within 7 days of culture, as we reasoned that the FBR is strongly influenced by early events in the first few days after implantation. Yet, it would be interesting to study also how the ECM proteins secreted by the involved cells in the FBR would be remodeled at longer culturing time up to 4–8 weeks, which is the typical time frame to obtain a TEBV with an in vivo bioreactor approach. In this respect, it would be also important to further dissect the specific types of collagens and GAGs (Table S1, Supporting Information) that are being produced by the cells depending on the released growth factor combination.[73] It would be also interesting to further optimize the LbL approach to allow a sequential release of the growth factors here studied. This could be achieved by incorporating the growth factors in different polyelectrolytes and by varying the polyelectrolyte configuration, so to impinge on the diffusion and erosion mechanism with which the release is governed in this system.

4. Conclusion

We have developed a delivery system to efficiently incorporate single and multiple GFs onto TEBV-inducing rods. Loaded GFs were released in a controlled manner for up to three weeks, maintaining their bioactivity. Addition of PDGF-$\beta\beta$ and IGF-1

in the TGF-β1 delivery system improved cellular proliferation rate, while TGF-β1 alone stimulated the highest myofibroblast differentiation. Though all GF releasing COX rods generally stimulated a significant increase in collagen and elastin, the release of TGF-β1 and IGF-1 provided the highest secretion and induced the highest GAG secretion per cell. When taking total ECM production, single PDGF-$\beta\beta$ and dual TGF-β1/PDGF-$\beta\beta$ releasing COX rods provided the highest collagen and elastin production. These promising results of altering cellular response and successful incorporation and release of single or multiple GFs provide a valuable tool for actively steering tissue formation for potential tissue engineering applications.

5. Experimental Section

Fabrication of PEOT/PBT Rods and Sheets: Polymeric rods were made of poly(ethylene oxide terephthalate)/poly(butylene terephthalate) (PEOT/PBT) – 300PEOT45PBT45, whereby a indicates the molecular weight in g mol^{-1} of the starting PEG blocks used in the copolymerization, while b and c represent the weight ratios of the PEOT and PBT blocks, respectively. The copolymer was kindly provided by Polyvation B.V. PEOT/PBT rods were fabricated from a Bioplotter device (Envisiontec GmbH), previously described by Moroni et al.[24] Briefly, PEOT/PBT granules were inserted into a syringe and heated at 180–200 °C. With a computer aided manufacturing software (CAM, PrimCAM), rods of 1.75 mm in diameter were extruded at 4–5 bars. Rods of ≈2 cm in length were used. PEOT/PBT sheets of 500 µm in thickness, made by a hot-embossed compression moulding technique as previously described,[4] were used as immunostaining samples. PEOT/PBT granules were distributed inside circular punched moulds, between two functionalized silicon wafers (FDTS, Sigma-Aldrich). The stack was positioned in the aperture of the temperature hydraulic press (Fortune Holland) and pressured at 10 bar and 180 °C for 5 min. Afterwards, the system was cooled to 60 °C and the pressure was released. The wafer and mould were manually separated to provide PEOT/PBT sheets of 1 cm in diameter. PEOT/PBT sheets were prepared for immunostaining studies.

Surface Modification and Activation: The surface of PEOT/PBT rods and sheets was modified to provide optimum surface area and roughness for cell attachment and proliferation, and activated for efficient loading GFs. Rods and sheets were etched with chloroform for 10 seconds. After etching, samples were rinsed with MilliQ water and sonicated two times for 15 min. Samples were then dried and oxygen plasma treated at a partial pressure of 100 mTorr and a power of 100 W for 5 min using a reactive ion etch system (Etch RIE Tetske, Nanolab, University Twente). All samples were sterilized by ethanol 70% for 30 min.

Mechanical Characterization: To measure the bending modulus of the rods, a 3-point bending mechanical set-up was used. Surface treated and untreated rods were tested following the DIN EN ISO 178 standard. Within the boundaries of the ISO standard, the speed in E-mod range was 1 mm min^{-1}, the speed after E-mod was 10 mm min^{-1}; the pre-load was 1N, and the maximum deformation was set to 15%.

Layer-by-Layer Incorporation of Single and Dual GFs: All chemicals were supplied by Sigma Aldrich, Germany. Single and dual incorporation of GFs were coated on PEOT/PBT rods and sheets. Single GF incorporation in the sequence of (PEI/PSS)$_2$(GF/HEP)$_4$PEI/PSS/PEI in which GF represents TGF-β1, PDGF-$\beta\beta$, and IGF-1 were similarly done as the final optimised procedure previously described.[20] Table 1 summarizes the LbL conditions and nomenclature used throughout the study. Briefly, polyethylenimine (PEI, M_w = 25 000) and poly(styrenesulfonate) (PSS, M_w = 70 000) were dissolved at 2 mg mL^{-1} in MilliQ water at a pH 3 and 10, respectively; while Heparin (HEP) at 1 mg mL^{-1} in NaCl 0.15 M at pH 9. Both polyelectrolytes were sterilized through a 0.02 µm filter. GFs (TGF-β1, PDGF-$\beta\beta$, IGF-1, RnD Systems) were kept sterile and dissolved in a 0.1% bovine serum albumin (BSA) 1x phosphate buffer solution (PBS) at pH 5 and concentrations 40, 40 and

Table 1. Overview of layer-by-layer (LbL) polyelectrolyte coating conditions of 300PEOT55PBT45 rods.

Nomenclature	Condition
(PEI/PSS)$_2$/(TGF-β1/HEP)$_4$PEI/PSS/PEI	Single growth factor (GF) release from LbL coating of 300PEOT55PBT45 where the GF is TGF-β1.
(PEI/PSS)$_2$/(PDGF-$\beta\beta$/HEP)$_4$PEI/PSS/PEI	Single growth factor (GF) release from LbL coating of 300PEOT55PBT45 where the GF is PDGF-$\beta\beta$.
(PEI/PSS)$_2$/(IGF-1/HEP)$_4$PEI/PSS/PEI	Single growth factor (GF) release from LbL coating of 300PEOT55PBT45 where the GF is IGF-1.
(PEI/PSS)$_2$/(TGF-β1/HEP/PDGF-$\beta\beta$/HEP)$_4$PEI/PSS/PEI	Dual growth factor (GF) release from LbL coating of 300PEOT55PBT45 where the GFs are TGF-β1 and PDGF-$\beta\beta$.
(PEI/PSS)$_2$/(IGF-1/HEP)$_4$PEI-(TGF-β1/HEP)$_4$PEI/PSS/PEI	Dual growth factor (GF) release from LbL coating of 300PEOT55PBT45 where the GFs are IGF-1 and TGF-β1.

500 ng mL^{-1}, respectively. All washing procedure used similar buffer as deposited polyelectrolytes and washed for 30 seconds in gently shaking. Deposition took place in Corning Costar Ultra-Low attachment multiwell plates (Sigma Aldrich) and Eppendorf LoBind Microcentrifuge Tubes: Protein (Fischer Scientific) pre-coated with PEI for PEI and GF deposition, or PSS for PSS and HEP deposition. A similar deposition procedure was used for dual GF incorporation, but with a sequence (TGF-β1/HEP/PDGF-$\beta\beta$/HEP)$_4$PEI/PSS/PEI and (IGF-1/HEP)$_4$PEI-(TGF-β1/HEP)$_4$PEI/PSS/PEI after the (PEI/PSS)$_2$ sequence. For all PDGF-$\beta\beta$ deposition, cold PDGF-$\beta\beta$ solution was used. All procedures were performed in a sterile fume hood.

Enzyme-Linked Immunosorbent Assay (ELISA): ELISA (n = 3) was conducted to quantify GF loading capacity and release rate profile. Loading capacity was measured by subtracting initial GF concentration to final concentration after deposition. For release rate profile, rods were incubated in PBS solution for 1, 3, 4, 6, 7, 9, 10, 12, 14, 16, 18, and 21 days. ELISA procedure was conducted according to the manufacturer's instructions (DuoSet ELISA development kit, R&D Systems Europe Ltd.).

Cell Expansion and Seeding: Human dermal fibroblasts (HDF, #R2320, ScienCell Research Laboratories) and neonatal rat dermal fibroblasts (nRDF, R106-05n, Tebu-bio Cell Application, Inc.) were cultured with basic culture medium comprising α-MEM (Gibco), fetal bovine serum (10%, Lonza), L-glutamine (2×10^{-3} M, Gibco) and penicillin (100 U mL^{-1}) and streptomycin (100 mg mL^{-1}, Gibco). nRDF were used as a cell model line, whereas HDF represent a closer cell population to the clinic. HDF and nRDF were expanded at initial seeding density of 5000 cells cm^{-2} and 3000 cells cm^{-2}, respectively. Culture was refreshed every 2–3 days. Upon 80–90% confluency, cells were harvested and trypsinized for cell seeding on the rods. A cell seeding density of 10000 cells mL^{-1} with at a volume of 250 µl was used, and culture medium was refreshed at day 1 and 4. All cell experiments were performed in a 5% CO$_2$ humid atmosphere at 37 °C.

Cell Proliferation and Glycosaminoglycans (GAGs) Assay: DNA assay was performed to assess cell proliferation at day 1, 4, and 7 with a CyQuant Cell Proliferation Assay kit (Molecular Probes). Proliferation study was evaluated up to day 7 to mimic what occurs in the body during FBR in the first week. Samples (n = 3) were washed gently with PBS twice, collected into a 500 µl Eppendorf tube and underwent three times freeze-thawing from −80 °C. Afterwards, samples were incubated for 1 h with 1x lysis buffer at room temperature (RT). Samples of day 4 and 7 underwent an additional overnight incubation in a Tris-EDTA buffered solution (1 mg mL^{-1} proteinase K, 18.5 lg mL^{-1} pepstatin A, and 1 lg mL^{-1} iodoacetamide, Sigma-Aldrich) at 56 °C. For all samples, an additional 1 h incubation with lysis buffer RNase was conducted. Next, CyQuant GR dye (1 ×) was mixed 1:1 with cell lysate in a black

96-well plate and incubated for 15 min in the dark. Fluorescence was measured using a spectrophotometer (VICTOR3 Multilabel Plate Reader, Perkin Elmer Corporation) at an excitation and emission wavelengths of 480 and 520 nm, respectively. GAGs assay was done by adding dimethylmethylene blue dye (DMMB, Sigma-Aldrich) to quantify sulfated glycosaminoglycans (sGAG)[25] of the remaining cell lysate and measured at 520 nm absorbance with a spectrophotometer (EL 312e Bio-TEK Instruments). Final quantification was calculated using a standard of chondroitin sulphate B (Sigma–Aldrich).

Sircol and Fastin Assay for Collagen and Elastin Content: Collagen samples ($n = 3$; both for HDF and nRDF seeded samples) at day 4 and 7 collected from cell cultured rods and supernatants underwent collagen extraction using cold acid pepsin (0.1 mg mL^{-1} 0.5 M acetic acid) and were left overnight at 4 °C. Collagen was isolated and concentrated before adding the Sircol Dye Reagent. The picosirius red-based colorimetric assay was performed according to the SirCol collagen dye binding assay kit (Biocolor Ltd.) and measured at 540 nm. Elastin samples ($n = 3$; both for HDF and nRDF seeded samples) at day 4 and 7 were collected from cell culture rods and supernatants. Insoluble elastin from cultured rods was first heated at 100 °C with oxalic acid (0.25 M) for 1 h to extract soluble α-elastin. Further elastin quantification was conducted following the Fastin elastin assay kit (Biocolor Ltd), and measured at 513 nm.

Scanning Electron Microscopy and Immunostaining: All chemicals were supplied by Sigma Aldrich, if not stated otherwise. Samples of rods and sheets ($n = 4$) were washed with PBS and fixed with 4% paraformaldehyde for 30 min at RT. After rinsing with PBS, rods ($n = 2$) underwent 70–80–90–100% dehydration steps of 30 min each. After dehydration, samples were critical point dried (CPD 030 Critical Point Dryer, Leica) and then gold sputtered for 30 seconds at 40 mA and 100 mTorr. The morphology of the cells was studied at 2500x magnification using a Philips XL30 ESEM-FEG SEM at 10 kV and a working distance of 10 mm.

Polymeric fixated sheets ($n = 2$), were permeabilized and blocked with TBP buffer (0.1% Triton X-100, 0.5% bovine serum albumin in PBS) overnight at 4 °C. Cells were stained with monoclonal anti-actin, α-smooth muscle actin (α-SMA, 1:200) conjugated with goat anti-mouse Alexa fluor 488 (Invitrogen, 1:1000), phalloidin-texas red (Molecular Probes, 1:100) and dapi (1:100). A three times washing steps with TBP buffer was done in between each staining incubation. Images were acquired using a Nanozoomer slide scanner equipped with a 40x objective (Hammamatsu). Cell morphology was also quantified by measuring their circularity. At least 20 cell images were taken for each condition in both SEM and fluorescence microscopy analysis.

Statistical Analysis: Statistical analysis were performed by Graphpad and expressed as mean ± s.d. Generally, assays were performed with triplicate biological sample, if not stated otherwise. Statistical analysis was done by Two-way Analysis of Variance (ANOVA) with Bonferroni's multiple comparison test ($p < 0.05$), unless otherwise indicated in the figure legends. For all figures the following applies: * = $p < 0.05$, ** = $p < 0.01$, *** = $p < 0.001$.

Supporting Information

Supporting Information is available from the Wiley Online Library or from the author.

Acknowledgements

Conflict of Interest

The authors declare no conflict of interest.

Data Availability Statement

The data that support the findings of this study are available from the corresponding author upon reasonable request.

Keywords

[1] J. M. Heddleston, M. Hitomi, M. Venere, W. A. Flavahan, K. Yang, Y. Kim, S. Minhas, J. N. Rich, A. B. Hjelmeland, *Curr. Pharm. Des.* **2011**, *17*, 2386.

[2] F. J. O'Brien, *Mater. Today* **2011**, *14*, 88.

[3] A. R. Amini, C. T. Laurencin, S. P. Nukavarapu, *Crit. Rev. Biomed. Eng.* **2012**, *40*, 363.

[4] F. F. Damanik, T. C. Rothuizen, C. van Blitterswijk, J. I. Rotmans, L. Moroni, *Sci. Rep.* **2014**, *4*, 6325.

[5] T. C. Rothuizen, F. F. Damanik, J. M. Anderson, T. Lavrijsen, M. A. Cox, T. J. Rabelink, L. Moroni, J. I. Rotmans, *Tissue Eng., Part C* **2015**, *21*, 436.

[6] T. C. Rothuizen, F. F. R. Damanik, T. Lavrijsen, M. J. T. Visser, J. F. Hamming, R. A. Lalai, J. Duijs, A. J. van Zonneveld, I. E. Hoefer, C. A. van Blitterswijk, T. J. Rabelink, L. Moroni, J. I. Rotmans, *Biomaterials* **2015**, *75*, 82.

[7] W. J. Geelhoed, K. E. A. van der Bogt, T. C. Rothuizen, F. F. R. Damanik, J. F. Hamming, C. D. Mota, M. S. van Agen, H. C. de Boer, M. T. Restrepo, B. Hinz, A. Kislaya, C. Poelma, A. J. van Zonneveld, T. J. Rabelink, L. Moroni, J. I Rotmans, *Biomaterials* **2020**, *229*, 119577.

[8] A. B. Roberts, M. B. Sporn, R. K. Assoian, J. M. Smith, N. S. Roche, L. M. Wakefield, U. I. Heine, L. A. Liotta, V. Falanga, J. H. Kehrl, *Proc. Natl. Acad. Sci. USA* **1986**, *83*, 4167.

[9] W. Lederle, H. J. Stark, M. Skobe, N. E. Fusenig, M. M. Mueller, *Am. J. Pathol.* **2006**, *169*, 1767.

[10] R. A. Achar, T. C. Silva, E. Achar, R. B. Martines, J. L. Machado, *Acta Cir. Bras.* **2014**, *29*, 125.

[11] D. F. Bowen-Pope, T. W. Malpass, D. M. Foster, R. Ross, *Blood* **1984**, *64*, 458.

[12] T. Kanzaki, K. Tamura, K. Takahashi, Y. Saito, B. Akikusa, H. Oohashi, N. Kasayuki, M. Ueda, N. Morisaki, *Arterioscler., Thromb., Vasc. Biol.* **1995**, *15*, 1951.

[13] L. M. Wakefield, T. S. Winokur, R. S. Hollands, K. Christopherson, A. D. Levinson, M. B Sporn, *J. Clin. Invest.* **1990**, *86*, 1976.

[14] C. H. Heldin, *Cell Commun. Signaling* **2013**, *11*, 97.

[15] J.- J. Lebrun, *ISRN Mol. Biol.* **2012**, *2012*, 1.

[16] H. Yu, *J. Natl. Cancer Inst.* **2000**, *92*, 1472.

[17] D. Alkekhia, P. T. Hammond, A. Shukla, *Annu. Rev. Biomed. Eng.* **2020**, *22*, 1.

[18] N. J. Shah, M. L. Macdonald, Y. M. Beben, R. F. Padera, R. E. Samuel, P. T Hammond, *Biomaterials* **2011**, *32*, 6183.

[19] S. Zhao, F. Caruso, L. Dähne, G. Decher, B. G. De Geest, J. Fan, N. Feliu, Y. Gogotsi, P. T. Hammond, M. C. Hersam,

A. Khademhosseini, N. Kotov, S. Leporatti, Y. Li, F. Lisdat, L. M. Liz-Marzán, S. Moya, P. Mulvaney, A. L. Rogach, S. Roy, D. G. Shchukin, A. G. Skirtach, M. M. Stevens, G. B. Sukhorukov, P. S. Weiss, Z. Yue, D. Zhu, W. J Parak, *ACS Nano* **2019**, *13*, 6151.

[20] F. F. R. Damanik, M. Brunelli, L. Pastorino, C. Ruggiero, C. van Blitterswijk, J. Rotmans, L. Moroni, *Biomater. Sci.* **2019**, *8*, 174.

[21] T. P. Richardson, M. C. Peters, A. B. Ennett, D. J. Mooney, *Nat. Biotechnol.* **2001**, *19*, 1029.

[22] R. R. Chen, E. A. Silva, W. W. Yuen, D. J. Mooney, *Pharm. Res.* **2007**, *24*, 258.

[23] A. Lamberg, G. Schmidmaier, K. Soballe, B. Elmengaard, *Acta Orthop.* **2006**, *77*, 799.

[24] L. Moroni, L. P. Lee, *J. Biomed. Mater. Res., Part A* **2009**, *88*, 644.

[25] D. M. Templeton, *Connect. Tissue Res.* **2009**, *17*, 23.

[26] R. E. Mooren, E. J. Hendriks, J. J. van den Beucken, M. A. Merkx, G. J. Meijer, J. A. Jansen, P. J. Stoelinga, *Tissue Eng., Part A* **2010**, *16*, 3159.

[27] P. T. Hammond, *Mater. Today* **2012**, *15*, 196.

[28] T. C. Rothuizen, F. F. R. Damanik, T. Lavrijsen, M. J. T. Visser, J. F. Hamming, R. A. Lalai, J. Duijs, A. J. van Zonneveld, I. E. Hoefer, C. A. van Blitterswijk, T. J. Rabelink, L. Moroni, J. I. Rotmans, *Biomaterials* **2016**, *75*, 82.

[29] T. Bezhaeva, W. J. Geelhoed, D. Wang, H. Yuan, E. P. van der Veer, C. Alem, F. F. R. Damanik, X. Qiu, A. V. Zonneveld, L. Moroni, S. Li, J. I. Rotmans, *Biomaterials* **2019**, *194*, 47.

[30] A. A. Deschamps, M. B. Claase, W. J. Sleijster, J. D. de Bruijn, D. W. Grijpma, J. Feijen, *J. Controlled Release* **2002**, *78*, 175.

[31] M. B. Claase, D. W. Grijpma, S. C. Mendes, J. D. De Bruijn, J. Feijen, *J. Biomed. Mater. Res., Part A* **2003**, *64*, 291.

[32] G. Singhvi, R. Singh, *Int. J. Pharm. Stud. Res.* **2011**, *II*, 77.

[33] T. Nandi, A. Rahman, N. Jahan, R. Islam, O. Pavel, *Spec. J. Med. Res. Health Sci.* **2017**, *2*, 8.

[34] K. E. Fischer, A. Jayagopal, G. Nagaraj, R. H. Daniels, E. M. Li, M. T. Silvestrini, T. A. Desai, *Nano Lett.* **2011**, *11*, 1076.

[35] M. Choi, K. G. Kim, J. Heo, H. Jeong, S. Y. Kim, J. Hong, *Sci. Rep.* **2015**, *5*, 17631.

[36] G. Ahuja, K. Pathak, *Indian J. Pharm. Sci.* **2009**, *71*, 599.

[37] G. Decher, J. B. Schlenoff, *Multilayer Thin Films*, Wiley-VCH Verlag GmbH & Co. KGaA, Weinheim, Germany **2012**. pp. 281–320.

[38] D. V. Volodkin, N. I. Larionova, G. B. Sukhorukov, *Biomacromolecules* **2004**, *5*, 1962.

[39] C. Wang, C. He, Z. Tong, X. Liu, B. Ren, F. Zeng, *Int. J. Pharm.* **2006**, *308*, 160.

[40] H.-P. Lim, *Particle Powder Bed Prop.* **2008**, *17*.

[41] M. S. Agren, H. H. Steenfos, S. Dabelsteen, J. B. Hansen, E. Dabelsteen, *J. Invest. Dermatol.* **1999**, *112*, 463.

[42] T. Nishiyama, N. Akutsu, I. Horii, Y. Nakayama, T. Ozawa, T. Hayashi, *Matrix* **1991**, *11*, 71.

[43] F. Strutz, M. Zeisberg, A. Renziehausen, B. Raschke, V. Becker, C. van Kooten, G. Müller, *Kidney Int.* **2001**, *59*, 579.

[44] H. Pratsinis, C. C. Giannouli, I. Zervolea, S. Psarras, D. Stathakos, D. Kletsas, *Wound Repair Regener.* **2004**, *12*, 374.

[45] L. Xiao, *Front. Biosci.* **2012**, *17*, 2667.

[46] N. Khalil, Y. D. Xu, R. O'Connor, V. Duronio, *J. Biol. Chem.* **2005**, *280*, 43000.

[47] S. Meran, D. W. Thomas, P. Stephens, S. Enoch, J. Martin, R. Steadman, A. O Phillips, *J. Biol. Chem.* **2008**, *283*, 6530.

[48] J. G. Simmons, J. B. Pucilowska, T. O. Keku, P. K Lund, *Am. J. Physiol.* **2002**, *283*, G809.

[49] D. Maroni, J. S. Davis, *Biol. Reprod.* **2012**, *87*, 127.

[50] A. Ghahary, E. E. Tredget, A. Ghahary, M. A. Bahar, C. Telasky, *Wound Repair Regener.* **2002**, *10*, 328.

[51] B. K. Lal, S. Saito, P. J. Pappas, F. T. PadbergJr, J. J. Cerveira, R. W. Hobson2nd, W. N. Durán, *J. Vascul. Surg.* **2003**, *37*, 1285.

[52] F. F. Damanik, M. Brunelli, C. van Blitterswijk, L. Moroni, *Sci. Rep.* **2014**, *4*, 1.

[53] K. Lee, E. A. Silva, D. J. Mooney, *J. R. Soc., Interface* **2011**, *8*, 153.

[54] R. Zhang, D. Ruan, C. Zhang, *J. Orthop. Surg. Res.* **2006**, *1*, 9.

[55] J. J. Tomasek, G. Gabbiani, B. Hinz, C. Chaponnier, R. A. Brown, *Nat. Rev. Mol. Cell Biol.* **2002**, *3*, 349.

[56] H. Yokoi, A. Sugawara, M. Mukoyama, K. Mori, H. Makino, T. Suganami, K. Yahata, Y. Fujinaga, I. Tanaka, K. Nakao, *Am. J. Kidney Dis.* **2001**, *38*, S134.

[57] C. Prante, H. Milting, A. Kassner, M. Farr, M. Ambrosius, S. Schön, D. G. Seidler, A. E. Banayosy, R. Körfer, J. Kuhn, K. Kleesiek, C. Götting, *J. Biol. Chem.* **2007**, *282*, 26441.

[58] J. E. Lee, S. E. Kim, I. C. Kwon, H. J. Ahn, H. Cho, S. H. Lee, H. J. Kim, S. C. Seong, M. C. Lee, *Artif. Organs* **2004**, *28*, 829.

[59] T. H. Alexander, A. B. Sage, A. C. Chen, B. L. Schumacher, E. Shelton, K. Masuda, R. L. Sah, D. Watson, *Tissue Eng., Part C* **2010**, *16*, 1213.

[60] G. van Osch, W. Marijnissen, S. W. van der Veen, H. L. Verwoerd-Verhoef, *Am. J. Rhinol.* **2001**, *15*, 187.

[61] D. H. Kim, P. P. Provenzano, C. L. Smith, A. Levchenko, *J. Cell Biol.* **2012**, *197*, 351.

[62] M. Ivarsson, A. McWhirter, T. K. Borg, K. Rubin, *Matrix Biol.* **1998**, *16*, 409.

[63] B. Hinz, *J. Invest. Dermatol.* **2007**, *127*, 526.

[64] J. J. Santiago, A. L. Dangerfield, S. G. Rattan, K. L. Bathe, R. H. Cunnington, J. E. Raizman, K. M. Bedosky, D. H. Freed, E. Kardami, I. M. Dixon, *Dev. Dyn.* **2010**, *239*, 1573.

[65] T. Daian, A. Ohtsuru, T. Rogounovitch, H. Ishihara, A. Hirano, Y. Akiyama-Uchida, V. Saenko, T. Fujii, S. Yamashita, *J. Invest. Dermatol.* **2003**, *120*, 956.

[66] G. R. Grotendorst, H. Rahmanie, M. R. Duncan, *FASEB J.* **2004**, *18*, 469.

[67] J. Baum, H. S. Duffy, *J. Cardiovasc. Pharmacol.* **2011**, *57*, 376.

[68] A. Patel, B. Fine, M. Sandig, K. Mequanint, *Cardiovasc. Res.* **2006**, *71*, 40.

[69] C. Saitow, D. L. Kaplan, J. J. Castellot, Jr, *Matrix Biol.* **2011**, *30*, 346.

[70] C. R. Kothapalli, A. Ramamurthi, *J. Tissue Eng. Regener. Med.* **2008**, *2*, 106.

[71] V. M. Kahari, D. R. Olsen, R. W. Rhudy, P. Carrillo, Y. Q. Chen, J. Uitto, *Lab. Invest.* **1992**, *66*, 580.

[72] P. P. Kuang, X. H. Zhang, C. B. Rich, J. A. Foster, M. Subramanian, R. H Goldstein, *Am. J. Physiol.* **2007**, *292*, L944.

[73] A. D. Theocharis, S. S. Skandalis, C. Gialeli, N. K. Karamanos, *Adv. Drug Delivery Rev.* **2016**, *97*, 4.